UDK: 624.31:005.001.26; 620.172.24
COSATI:20-11
doi: 10.5937/str2201003P

Analysis and Optimization of the Main Girder of the Bridge Crane with an Asymmetric Box Cross-Section

Goran Pavlović [1)]
Mile Savković [2)]

The presented research deals with the optimal design of the main girder with an asymmetric box cross-section of the double-beam bridge crane. The Moth-Flame Optimization algorithm (MFO) is used for solving this multicriteria optimization problem. This algorithm is a relatively new population-based metaheuristic method. The paper takes the following criteria as the constraint functions: strength, local stability of the girder plates (webs and top flange), local stability of the longitudinal stiffeners, global stability of the main girder, deflections, and period of oscillation. The justification of the proposed procedure is shown in one example of a real solution of the double-beam bridge crane. Significant savings in material were achieved in this research, within the range of 19.42 to 25.49%. The use of this algorithm enables the application of a very large number of variables and constraint functions, whereby the optimal values are obtained in a relatively short period.

Key words: **Double-beam bridge crane, Asymmetric box cross-section, Optimal design, Metaheuristic.**

Introduction

DOUBLE-BEAM bridge cranes are used for lifting and transporting heavy loads from one location to another. They are most frequently applied in production halls, industrial plants, etc., for manipulation, servicing and maintenance.

The lightweight design of the main girder of the double-beam bridge crane is the most important engineering task. The main girder is the most responsible part of the double-beam bridge crane. The weight of the main girder has the largest share in the total weight of the whole bridge crane structure, so it is very important to perform its optimization in order to reduce the total weight of the double-beam bridge crane. Proper choice of the geometric parameters of the box-girder (and its auxiliary constructive elements) leads to a significant reduction in the weight of the girder, as evidenced by numerous studies.

The paper [1] shows the position of the longitudinal stiffeners on the optimal geometric parameters of the box girder of bridge cranes. Generalized Reduced Gradient (GRG2) code was used as the optimization method. Placement of auxiliary constructive elements (such as longitudinal and transverse stiffeners) influences the improvement of the structure of the box girder in terms of savings in material up to 38.3% [2]. The optimization of the bridge crane's box girder performed in the paper [3] showed that regular placement of the longitudinal stiffeners may result in savings from 18 to 21%.

The use of various metaheuristic optimization algorithms is very present in solving engineering problems. The authors [4] presented the application of the Cyclical Parthenogenesis Algorithm (CPA) in optimizing the welded girder of the crane runway beam. The paper [5] presented the application of three metaheuristic optimization algorithms to minimize the weight of the box-girder of bridge cranes. The paper [6] considered the problem of optimizing the dimensions of the box cross-section of the double-beam bridge crane (using the Adaptive Genetic Algorithm). The paper [7] presented the application of the Harris Hawks Optimizer (HHO) method on some engineering problems, where the results were compared with the previous ones.

In this research, one bio-inspired optimization algorithm (MFO) is applied for a multicriteria optimization problem, to reduce the weight of the main girder of the double-beam bridge crane (with an asymmetric box cross-section).

The aim of this research is to present the analysis and optimization of an asymmetrical box cross-section of the main girder of the double-beam bridge crane, whereby the longitudinal stiffeners are also subject to optimization, which can be easily cold-formed to the obtained dimensions.

The optimization problem

The purpose of this paper is to minimize the cross-sectional area of the main girder of the double-beam bridge crane with an asymmetric box cross-section. It means determining its optimal geometric parameters, while all constraint functions and recommendations must be satisfied.

[1)] University of Niš, Faculty of Electronic Engineering, 18000 Niš, SERBIA
[2)] University of Kragujevac, Faculty of Mechanical and Civil Engineering in Kraljevo, SERBIA
Correspondence to: Goran Pavlović, e-mail: goran.pavlovic@elfak.ni.ac.rs

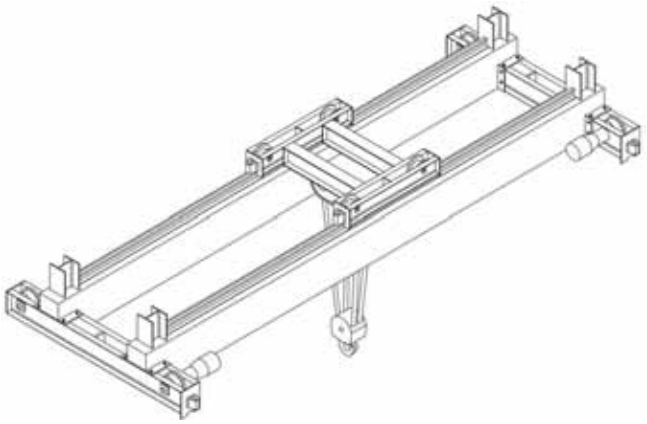

Figure 1. The structure of the double-beam bridge crane

Fig.1 presents the general view of a double-beam bridge crane structure, [8]. This figure shows the appearance of the bridge crane carrying structure, which consists of the two main girders, the electrical trolley, as well as of electrical end carriages.

The mathematical formulation of the optimization problem

It is a single-objective multicriteria optimization problem, and it can be defined in the following way:

$$\min f_{obj}(X) \;\; subject\ to \;\; g_i(X) \le 0 \tag{1}$$

and

$$l_j \le x_j \le u_j \tag{2}$$

where $f_{obj}(X)$ is the objective function, $g_i(X)$ are constraint functions, i=1,..,m is the number of constraints, j=1,..,n is the number of design variables, X is the design vector made of n variables, l_j is the lower limit, and u_j is the upper limit.

Variables (x_j) are values that should be defined during the optimization process. This research treats ten optimization variables (Fig.2):

$$\begin{aligned} X &= \left[x_1\ x_2\ x_3\ x_4\ x_5\ x_6\ x_7\ x_8\ x_9\ x_{10}\right]^T = \\ &= \left[t_1\ t_2\ t_3\ t_4\ b_1\ h\ v\ b_p\ h_p\ t_p\right]^T \end{aligned} \tag{3}$$

Input parameters for this optimization problem are: Classification class, Q is the carrying capacity of the bridge crane, L is the span of the bridge crane, m_t is the weight of the trolley, b_t is the distance between wheels of the trolley, e_1 is the distance between wheel 1 and resulting force in the vertical plane (Fig.3), a_m is the bridge crane acceleration, E is the elastic modulus of the plate, ρ is the density of the girder material, R_{e1} is the minimum yield stress of the plate material, and R_{e2} is the minimum yield stress of the longitudinal stiffeners.

The objective function

The cross-sectional area of an asymmetric box cross-section of the main girder of the double-beam bridge crane (the objective function) f_{obj} (Fig.2) is noted as:

$$f_{obj} = A + 2 \cdot A_L \tag{4}$$

where A is the area of an asymmetric box (webs, bottom and top flanges), and A_L is the area of the longitudinal stiffener:

$$A = b \cdot t_1 + b_2 \cdot t_2 + h \cdot (t_3 + t_4) \tag{5}$$

$$A_L = t_p \cdot (b_p + h_p) \tag{6}$$

Materials S355, S275 and S235 will be analyzed for the cross-sectional area A, while only S235 will be considered for A_L, as it is a constructive element of the main girder.

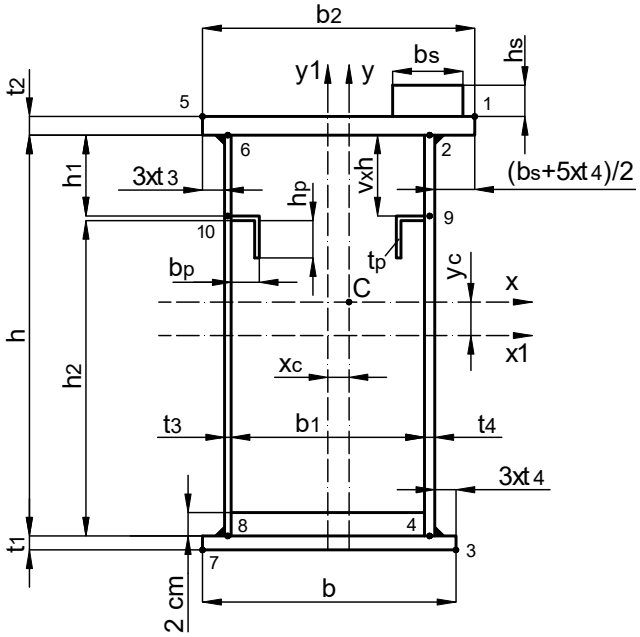

Figure 2. The cross-section of the main girder of the double-beam bridge crane

For the load capacity of the observed example of a bridge crane, a rail with dimensions 6 *cm* x 4 *cm*, was adopted (A_s).

All dimensions and coordinates from Fig.2 are marked and defined. It should be noted that the position coordinates are shown in relation to the *x-y* coordinate system and as such were used in this analysis. Due to the asymmetry, as well as the shape and dimensions of the plates, the main coordinate system is rotated at a very small angle, but such a value is almost negligible. In order to achieve this and avoid the influence of oblique bending, this rotation (α) should be less than 1°:

$$g_1 = |\alpha| - 1° = \left| \frac{90°}{\pi} \cdot atg\left(\frac{-2 \cdot I_{xy}}{I_x - I_y} \right) \right| - 1° \le 0 \tag{7}$$

All necessary geometrical dimensions, coordinates, and properties (x_c, y_c, I_x, I_y, I_{xy}, W_x, W_y, S_x, A^*…) in any characteristic point of the cross-section can be calculated using well-known expressions.

The calculation model of the main girder of the double-beam bridge crane

The following figure shows a model of a simple beam (a model of a bridge crane's main girder) with all loads (Fig.3). Determination of all static quantities is done in compliance with [9]. The meaning and calculation of all these static quantities are defined in the mentioned literature (q, e_2, F_1, F_2, k_a, F_{1h}, F_{2h}, $F_{1,st}$, F_v, F_t, M_v, M_h, z_1, M_{tA}, and γ).

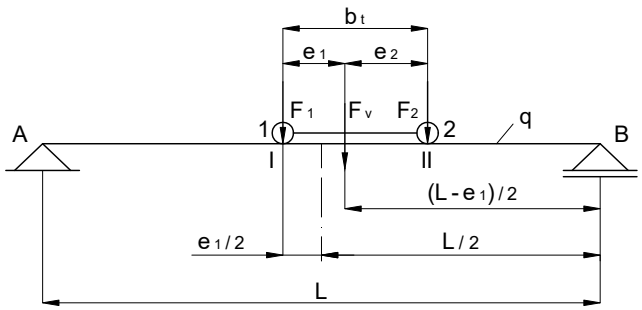

Figure 3. Loads of the main girder of the double-beam bridge crane

The criterion of strength

When calculating the maximum stresses in the characteristic points of the box cross-section, situations are observed when the highest possible loads occur, in place *I* (Fig.2) [9]. This primarily refers to the horizontal plane, since due to the movement of the bridge crane in the horizontal direction, an inertial force occurs, so that both the left and right sides of the cross-section of the main girder can be tensile or compressed. As the main girder is asymmetric with the rail above one vertical plate, this is of a great importance for the analysis. It is present in case of local stability, for compressed plates and longitudinal stiffener, too. In addition to the main bending stresses in both planes, local stress from the trolley wheel pressure was also analyzed. The tangential stresses were taken into account, too, [9].

Maximum stresses in the characteristic points of the box-section (Fig.2) must be lower than permissible stresses (σ_d, τ_d) [9]. For this criterion, the constraint functions are:

$$g_2 = \sigma_{1u} - \sigma_d = \frac{M_v}{W_{1x}} + \frac{M_h}{W_{1y}} - \sigma_d \le 0 \tag{8}$$

$$g_3 = \sigma_{2z} - \sigma_d = \frac{M_v}{W_{2x}} + \frac{M_h}{W_{2y}} - \sigma_d \le 0 \tag{9}$$

$$g_4 = \sigma_y - \sigma_d = \frac{\gamma \cdot F_1}{t_4 \cdot z_1} - \sigma_d \le 0 \tag{10}$$

$$g_5 = \tau_2 - \tau_d = \frac{F_t \cdot S_{2x}}{I_x \cdot (t_3 + t_4)} + \frac{M_{tA}}{A^* \cdot (t_3 + t_4)} - \tau_d \le 0 \tag{11}$$

$$g_6 = \sigma_{2u} - \sigma_d = \\ = \sqrt{{\sigma_{2z}}^2 + {\sigma_y}^2 - \sigma_{2z} \cdot \sigma_y - 3 \cdot {\tau_2}^2} - \sigma_d \le 0 \tag{12}$$

$$g_7 = \sigma_{3u} - \sigma_d = \frac{M_v}{W_{3x}} + \frac{M_h}{W_{3y}} - \sigma_d \le 0 \tag{13}$$

$$g_8 = \sigma_{5u} - \sigma_d = \frac{M_v}{W_{5x}} + \frac{M_h}{W_{5y}} - \sigma_d \le 0 \tag{14}$$

$$g_9 = \sigma_{7u} - \sigma_d = \frac{M_v}{W_{7x}} + \frac{M_h}{W_{7y}} - \sigma_d \le 0 \tag{15}$$

Stresses at all points of the box cross-section were not considered, but only at those where the highest stresses occur.

The criterion of local stability of top plate

Checking the local stability of top plate (length $2 \cdot h$, width b_1 and thickness t_2) is performed according to [10]. The constraint functions are:

$$g_{10} = \sigma_{1p} - \sigma_{1pd} = \nu_1 \cdot \left(\frac{M_v}{W_{1x}} + \frac{M_h}{W_{2y}} \right) - c_{1p} \cdot \chi_{1p} \cdot R_{e1} \le 0 \tag{16}$$

$$g_{11} = \sigma_{1p} - R_{e1} = \nu_1 \cdot \left(\frac{M_v}{W_{1x}} + \frac{M_h}{W_{2y}} \right) - R_{e1} \le 0 \tag{17}$$

$$g_{12} = \sigma_{2p} - \sigma_{2pd} = \nu_1 \cdot \left(\frac{M_v}{W_{1x}} + \frac{M_h}{W_{6y}} \right) - c_{2p} \cdot \chi_{2p} \cdot R_{e1} \le 0 \tag{18}$$

$$g_{13} = \sigma_{2p} - R_{e1} = \nu_1 \cdot \left(\frac{M_v}{W_{1x}} + \frac{M_h}{W_{6y}} \right) - R_{e1} \le 0 \tag{19}$$

where ν_1 is load case 1 factored load coefficient, according to [9], c_{1p}, c_{2p}, χ_{1p}, and χ_{2p} are coefficients, according to [10].

The criterion of local stability of the webs

It is necessary to check local stability of the webs above the longitudinal stiffener (length $2 \cdot h$, height h_1 and thickness t_3 and t_4) as well as local stability of the webs plate under the longitudinal stiffener (length $2 \cdot h$, height h_2 and thickness t_3 and t_4).

Checking the local stability of the webs (t_4) is performed according to [11]. Constraint functions have the following form:

$$g_{14} = \nu_1 \cdot \left[\frac{\left(\frac{M_v}{W_{2x}} + \frac{M_h}{W_{2y}} \right)}{\sigma_{kr1}} + \frac{\sigma_y}{\sigma_{Mkr1}} \right] + \\ + \left[\nu_1 \cdot \frac{\frac{F_t}{h \cdot (t_3 + t_4)} + \frac{M_{tA}}{A^* \cdot (t_3 + t_4)}}{\tau_{kr1}} \right]^2 - 0.9 \le 0 \tag{20}$$

$$g_{15} = \nu_1 \cdot \left[\frac{\left(\frac{M_v}{W_{9x}} + \frac{M_h}{W_{9y}} \right)}{\sigma_{kr2}} + \frac{0.4 \cdot \sigma_y}{\sigma_{Mkr2}} \right] + \\ + \left[\nu_1 \cdot \frac{\frac{F_t}{h \cdot (t_3 + t_4)} + \frac{M_{tA}}{A^* \cdot (t_3 + t_4)}}{\tau_{kr2}} \right]^2 - 1 \le 0 \tag{21}$$

where σ_{kr1}, σ_{Mkr1} and τ_{kr1} are critical stresses for the web above the longitudinal stiffener, σ_{kr2}, σ_{Mkr2}, τ_{kr2} are critical stresses for the web under the longitudinal stiffener, according to [11].

Checking the local stability of the webs (t_3) is performed according to [10]. Constraint functions have the following form:

$$g_{16} = \sigma_{1w} - \sigma_{1wd} = \nu_1 \cdot \left(\frac{M_v}{W_{6x}} - \frac{M_h}{W_{6y}} \right) - c_{1w} \cdot \chi_{1w} \cdot R_{e1} \le 0 \tag{22}$$

$$g_{17} = \sigma_{1w} - R_{e1} = \nu_1 \cdot \left(\frac{M_v}{W_{6x}} - \frac{M_h}{W_{6y}} \right) - R_{e1} \le 0 \quad (23)$$

$$g_{18} = \sigma_{2w} - \sigma_{2wd} = \\ = \nu_1 \cdot \left(\frac{M_v}{W_{6x}} + \frac{M_h}{W_{6y}} \right) - c_{2w} \cdot \chi_{2w} \cdot R_{e1} \le 0 \quad (24)$$

$$g_{19} = \sigma_{2w} - R_{e1} = \nu_1 \cdot \left(\frac{M_v}{W_{6x}} + \frac{M_h}{W_{6y}} \right) - R_{e1} \le 0 \quad (25)$$

$$g_{20} = \sigma_{3w} - \sigma_{3wd} = \\ = \nu_1 \cdot \left(\frac{M_v}{W_{10x}} - \frac{M_h}{W_{10y}} \right) - c_{3w} \cdot \chi_{3w} \cdot R_{e1} \le 0 \quad (26)$$

$$g_{21} = \sigma_{3w} - R_{e1} = \nu_1 \cdot \left(\frac{M_v}{W_{10x}} - \frac{M_h}{W_{10y}} \right) - R_{e1} \le 0 \quad (27)$$

$$g_{22} = \sigma_{4w} - \sigma_{4wd} = \\ = \nu_1 \cdot \left(\frac{M_v}{W_{10x}} + \frac{M_h}{W_{10y}} \right) - c_{4w} \cdot \chi_{4w} \cdot R_{e1} \le 0 \quad (28)$$

$$g_{23} = \sigma_{4w} - R_{e1} = \nu_1 \cdot \left(\frac{M_v}{W_{10x}} + \frac{M_h}{W_{10y}} \right) - R_{e1} \le 0 \quad (29)$$

where c_{1w}, c_{2w}, χ_{1w} and χ_{2w}, are coefficient for the web above the longitudinal stiffener, c_{3w}, c_{4w}, χ_{3w}, and χ_{4w} are coefficient for the web under the longitudinal stiffener, according to [10].

The criterion of global stability of the main girder

The verification of global stability, in this case, is performed based on standards [12-14]. Constraint functions, in this case, have the following form:

$$g_{24} = \sigma_b - \sigma_{bd} = \nu_1 \cdot \frac{M_v}{W_{1x}} - \chi_b \cdot R_{e1} \le 0 \quad (30)$$

$$g_{25} = \frac{2 \cdot b_1 + t_3 + t_4}{2 \cdot t_2} - 1.33 \cdot \sqrt{\frac{E}{R_{e1}}} \le 0 \quad (31)$$

$$g_{26} = \frac{6 \cdot t_4 + b_s}{2 \cdot t_2} - 0.454 \cdot \sqrt{\frac{E}{R_{e1}}} \le 0 \quad (32)$$

$$g_{27} = \frac{2 \cdot h + t_1 + t_2}{2 \cdot b_1 + t_3 + t_4} - 10 \le 0 \quad (33)$$

where χ_b is a non-dimensional coefficient, according to [12].

The criterion of local stability of the longitudinal stiffeners

The verification of local stability of the longitudinal stiffeners is performed according to standards [10] and [12]. Constraint functions have the following form:

$$g_{28} = \sigma_{l1} - \sigma_{kr3} = \nu_1 \cdot \left(\frac{M_v}{W_{9x}} + \frac{M_h}{W_{9y}} \right) - \chi_1 \cdot R_{e2} \le 0 \quad (34)$$

$$g_{29} = \sigma_{l2} - \sigma_{kr4} = \nu_1 \cdot \left(\frac{M_v}{W_{10x}} + \frac{M_h}{W_{10y}} \right) - \chi_2 \cdot R_{e2} \le 0 \quad (35)$$

$$g_{30} = \frac{b_p}{t_p} - 0.665 \cdot \sqrt{\frac{K_\sigma \cdot E}{R_{e2}}} \le 0 \quad (36)$$

where χ_1, χ_2, and K_σ are coefficient, according to [12].

The criterion of oscillation

With this criterion, the relaxation time (T) of oscillations of the weight (m_1), located in the middle of the main girder, must be checked. The analysis procedure was performed in compliance with [9] The constraint function has the following form:

$$g_{31} = T - T_d = \pi \cdot \sqrt{\frac{m_1 \cdot L^3}{12 \cdot B_x}} \cdot \frac{\ln(20)}{\gamma_d} - T_d \le 0 \quad (37)$$

$$m_1 = \frac{Q + m_t}{2} + 1.1 \cdot 0.486 \cdot \rho \cdot \left(A_s + A + 2 \cdot A_L \right) \cdot L \quad (38)$$

where B_x is the flexural rigidity in x-direction, γ_d is the logarithmic decrement, and T_d is the permissible time of damping of oscillation, according to [9]. The weight is increased by 10 % due to diaphragms, auxiliary constructive elements and welded connections, eq. 38.

The criterion of stiffness

This criterion analyses deflections in the vertical and horizontal plane. The total deflections in both planes ($f_{u,v}$,$f_{u,h}$) must be lower than the permissible ones ($f_{dop,v}$, $f_{dop,h}$), according to [9].

$$f_{u,v} = \frac{F_{1,st} \cdot L^3}{24 \cdot B_x} \cdot \left[1 - 3 \cdot \left(\frac{b_t}{L} \right)^2 \right] + \\ + \frac{5 \cdot q \cdot L^4}{384 \cdot B_x} \le f_{dop,v} = K_v \cdot L \quad (39)$$

$$f_{u,h} = \frac{k_a \cdot F_{1,st} \cdot L^3}{24 \cdot B_y} \cdot \left[1 - 3 \cdot \left(\frac{b_t}{L} \right)^2 \right] + \\ + \frac{5 \cdot k_a \cdot q \cdot L^4}{384 \cdot B_y} \le f_{dop,h} = K_h \cdot L \quad (40)$$

The constraint functions, based on Eqs. (39, 40) are:

$$g_{32} = f_{u,v} - f_{dop,v} \le 0 \quad (41)$$

$$g_{33} = f_{u,h} - f_{dop,h} \le 0 \quad (42)$$

where B_y is the flexural rigidity in y-direction, K_v and K_h are the coefficient that depends on Classification class (the purpose of the bridge crane and control condition), according to [9].

The optimization method

In this research, the Moth-Flame Optimization algorithm (MFO) is chosen for solving this multicriteria constrained optimization problem. MFO is very effective for solving real engineering problems, [15].

The Moth-Flame Optimization algorithm is a population-based bio-inspired algorithm, first introduced by Mirjalili,

[15]. This metaheuristic algorithm is based on the computer simulation of the navigation of moths. The main inspiration of this algorithm is the navigation method of moths in nature called transverse orientation. Moths fly by night by maintaining a fixed angle with respect to the moon, a very effective mechanism for flying in a straight line for long distances. They have been evolved to fly by night using the moonlight, where a moth flies by maintaining a fixed angle concerning the moon. Moths fly spirally around the lights because they are tricked by artificial lights. However, these insects are trapped in a useless or deadly spiral path around artificial lights [15].

The pseudocode for this metaheuristic algorithm of optimization is shown in [15]. MATLAB code for this metaheuristic algorithm of optimization, in original form, without any modifications and hypbridization, is taken according to [16].

Results of optimization

The optimization process is performed based on the MFO method, using MATLAB.

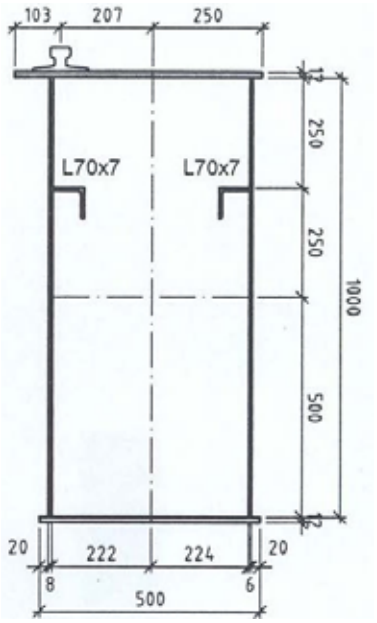

Figure 4. Cross-section of the main girder for the observed crane example

Fig.4 shows a cross-section of the main girder of the existing solution double-beam bridge crane, located at the Impol Seval company, Serbia. All measurements in the mentioned figure are in millimeters.

Table 1 shows the project data of the double-beam bridge crane that are in exploitation. These data also represent the input parameters for the optimization process, where A_{pr} represents the cross-sectional area of the box cross-section. Other data are taken from [9], depending on the Classification class.

Table 1. Technical parameters of the double-beam crane

Q (t)	L (m)	m_t (t)	b_t (cm)	Cl. class	a_m (m/s^2)	Re (kN/cm^2)	b_s (cm)	h_s (cm)	A_{pr} (cm^2)
20	22.5	6.4	320	2	0.2	35.5	6	4	286

The control parameters of the MFO algorithm used for each example solved in this paper are:

- N_{pop} = 200 - population size, and max_it = 500 - maximum number of iterations.

Constraints related to the minimum sheet thickness and other dimensions of constructive and technological character are taken through the lower and upper values of the variables.

Bound values of variables for all bridge cranes are:

$$0.6 \le t_1, \quad t_2 \le 3, \quad 0.5 \le t_3, \quad t_4 \le 2, \quad 20 \le b_1 \le 50,$$

$$60 \le h \le 150, \; 1/5 \le v \le 1/3, \; 3 \le b_p \le 10,$$

$$2.5 \le h_p \le 8, \; 0.3 \le t_p \le 1.$$

By applying the MFO optimization procedure, the optimal geometric parameters, the values of the optimal areas, material savings, as well as the characteristics of the optimization procedure are obtained (Tables 2-10).

Presented results of this research (Tables 2-10 and convergence diagrams) are taken from two of the conducted repetitions from the optimization process Variant 1 and Variant 2), for all types of materials.

Table 2 presents the characteristics of the optimization process for the two chosen variants, for S355. Table 3 presents the optimal values of the variables for the two chosen variants, for S355. Table 4 presents the rounded values of the optimal geometric parameters, optimal areas, and material savings for the two chosen variants, for S355.

Table 2. Characteristics of the optimization process, S355

V.	Best (cm^2)	Worst (cm^2)	Mean (cm^2)	Std (-)	time (s)
1	204.58	413.93	211.42	23.60	16.03
2	204.00	382.18	209.24	18.47	13.35

Table 3. The optimal values of the variables, S355

V.	x_1 (cm)	x_2 (cm)	x_3 (cm)	x_4 (cm)	x_5 (cm)	x_6 (cm)	x_7 (-)	x_8 (cm)	x_9 (cm)	x_{10} (cm)
1	0.600	1.171	0.500	0.516	34.25	123.23	0.2477	6.175	2.500	0.476
2	0.600	1.506	0.513	0.514	26.94	122.89	0.2522	6.185	2.500	0.477

Table 4. The rounded values of the optimal geometric parameters, optimal areas, and material savings, S355

V.	t_1 (cm)	t_2 (cm)	t_3 (cm)	t_4 (cm)	b_1 (cm)	h (cm)	b_p (cm)	h_p (cm)	t_p (cm)	A_o (cm^2)	Saving (%)
1	0.6	1.2	0.5	0.6	34.3	123.2	6.2	2.5	0.5	217.12	24.08
2	0.6	1.6	0.6	0.6	27.0	122.9	6.2	2.5	0.5	230.46	19.42

The following graphs show the convergence diagrams for both variants, for S355 (Figs.5, 6).

Table 5 presents the characteristics of the optimization process for the two chosen variants, for S275. Table 6 presents the optimal values of the variables for the two chosen variants, for S275. Table 7 presents the rounded values of the optimal geometric parameters, optimal areas, and material savings for the two chosen variants, for S275.

Table 5. Characteristics of the optimization process, S275

V.	Best (cm^2)	Worst (cm^2)	Mean (cm^2)	Std (-)	time (s)
1	209.95	304.78	214.61	15.38	15.97
2	209.34	336.10	213.13	14.34	15.98

Table 6. The optimal values of the variables, S275

V.	x_1 (cm)	x_2 (cm)	x_3 (cm)	x_4 (cm)	x_5 (cm)	x_6 (cm)	x_7 (-)	x_8 (cm)	x_9 (cm)	x_{10} (cm)
1	0.600	1.577	0.500	0.508	30.90	122.82	0.2554	4.959	2.500	0.382
2	0.600	1.754	0.500	0.522	27.02	122.65	0.2656	4.669	3.657	0.360

Table 7. The rounded values of the optimal geometric parameters, optimal areas, and material savings, S275

V.	t_1 (cm)	t_2 (cm)	t_3 (cm)	t_4 (cm)	b_1 (cm)	h (cm)	b_p (cm)	h_p (cm)	t_p (cm)	A_o (cm^2)	Saving (%)
1	0.6	1.6	0.5	0.6	30.9	122.8	5.0	2.5	0.4	223.06	22.01
2	0.6	1.8	0.5	0.6	27.0	122.7	4.7	3.7	0.4	221.91	22.41

The following graphs show the convergence diagrams for both variants, for S275 (Figs.7, 8).

Table 8 presents the characteristics of the optimization process for the two chosen variants, for S235.

Table 8. Characteristics of the optimization process, S235

V.	Best (cm^2)	Worst (cm^2)	Mean (cm^2)	Std (-)	time (s)
1	211.59	332.42	221.17	19.16	15.95
2	212.13	321.81	218.98	17.76	16.99

Table 9 presents the optimal values of the variables for the two chosen variants, for S235.

Table 9. The optimal values of the variables, S235

V.	x_1 (cm)	x_2 (cm)	x_3 (cm)	x_4 (cm)	x_5 (cm)	x_6 (cm)	x_7 (-)	x_8 (cm)	x_9 (cm)	x_{10} (cm)
1	0.609	0.969	0.575	0.554	35.62	123.42	0.2634	5.220	2.500	0.402
2	0.600	1.075	0.543	0.544	38.18	123.33	0.2631	4.862	2.667	0.374

Table 10 presents the rounded values of the optimal geometric parameters, optimal areas, and material savings for the two chosen variants, for S235.

Table 10. The rounded values of the optimal geometric parameters, optimal areas, and material savings, S235

V.	t_1 (cm)	t_2 (cm)	t_3 (cm)	t_4 (cm)	b_1 (cm)	h (cm)	b_p (cm)	h_p (cm)	t_p (cm)	A_o (cm^2)	Saving (%)
1	0.7	1.0	0.6	0.6	35.6	123.4	5.2	2.5	0.4	225.62	21.11
2	0.6	1.1	0.6	0.6	28.2	123.3	4.9	2.7	0.4	213.11	25.49

The following graphs show the convergence diagrams for both variants, for S235 (Figures 9 and 10).

Based on the obtained results, it is noticed that with the decrease of the value for R_{el} of the sheet metal material of the box cross-section, there is no significant change in the value of the optimal cross-sectional area. The recalculated values of these surfaces (due to taking round values of sheet thickness) give the possibility to choose the most favourable variant, depending on the dimensions and type of the material (R_{el}).

Conclusion

This paper presents the analysis and optimal design of the main girder of the double-beam bridge crane with an asymmetric box cross-section, using the MFO optimization method, according to national standards. The criteria of permissible stresses, local stability of the girder plates (webs and top flange), local stability of the longitudinal stiffeners, global stability of the main girder, deflections, and period of oscillation were applied as the constraint functions. The target (objective) function is the cross-sectional area shown in Fig.2.

The results obtained in this paper show the justification in the application of the proposed form of asymmetric box cross-section, as well as the model of analysis and optimization, which is reflected in the material savings in the range of 19.42-25.49 % (Tables 4, 7, 10). Also, in this analysis, it was adopted that the distance between the diaphragms is $2 \cdot h$ (which is more than 245 *cm* based on the obtained results), while in the observed example, this value is 150 *cm*, so that savings were made in this as well.

The MFO method used in a relatively short time (Tables 2, 5, 8) came to the optimal solution usually after 200-250 iterations, bearing in mind that there were 10 variables and 33 constraint functions (Figs.5-10).

The presented philosophy of an optimal design to achieve light carrying structures, and the application of the presented MFO method, as a metaheuristic optimization method, enables the implementation of this procedure for similar types of carrying structures, where a large number of variables and constraint functions can be applied. This helps designers to get preliminary results in the first phase of design quickly and easily.

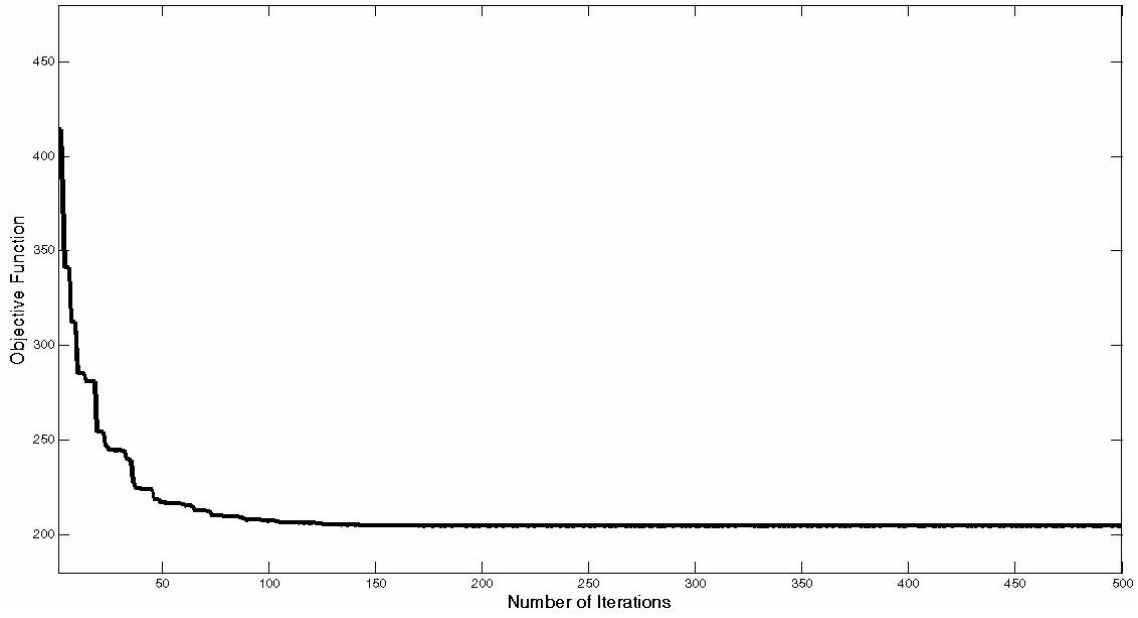

Figure 5. Convergence diagram for Variant 1, S355

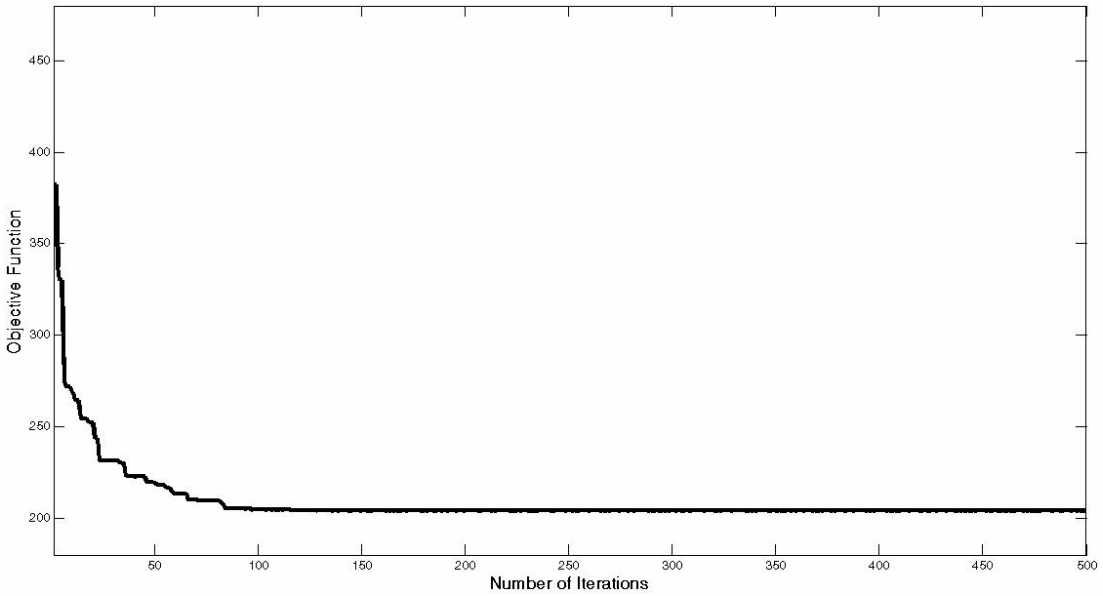

Figure 6 Convergence diagram for Variant 2, S355

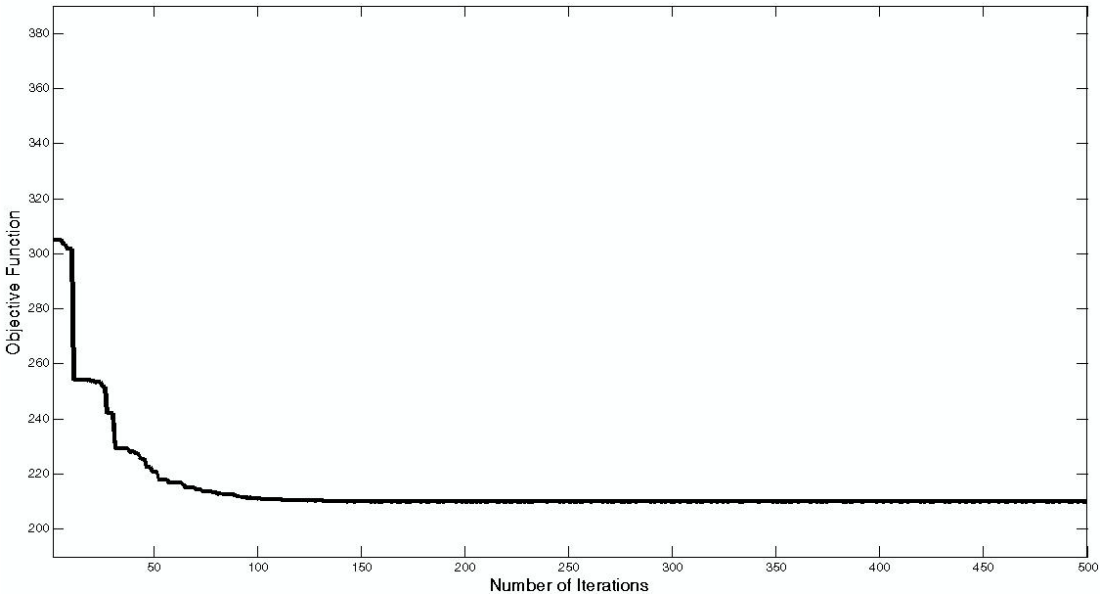

Figure 7. Convergence diagram for Variant 1, S275

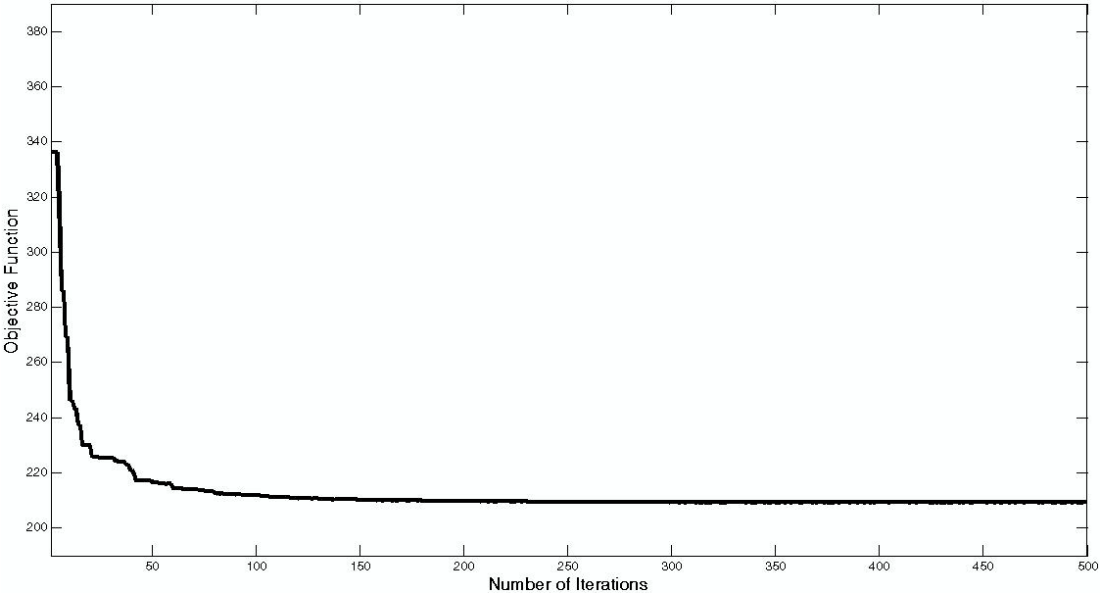

Figure 8. Convergence diagram for Variant 2, S275

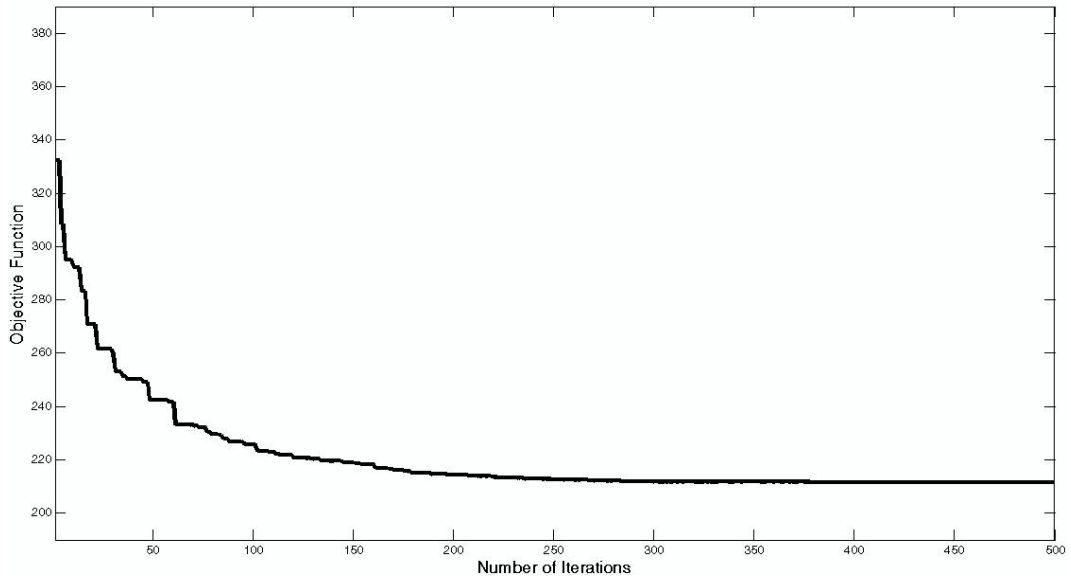

Figure 9. Convergence diagram for Variant 1, S235

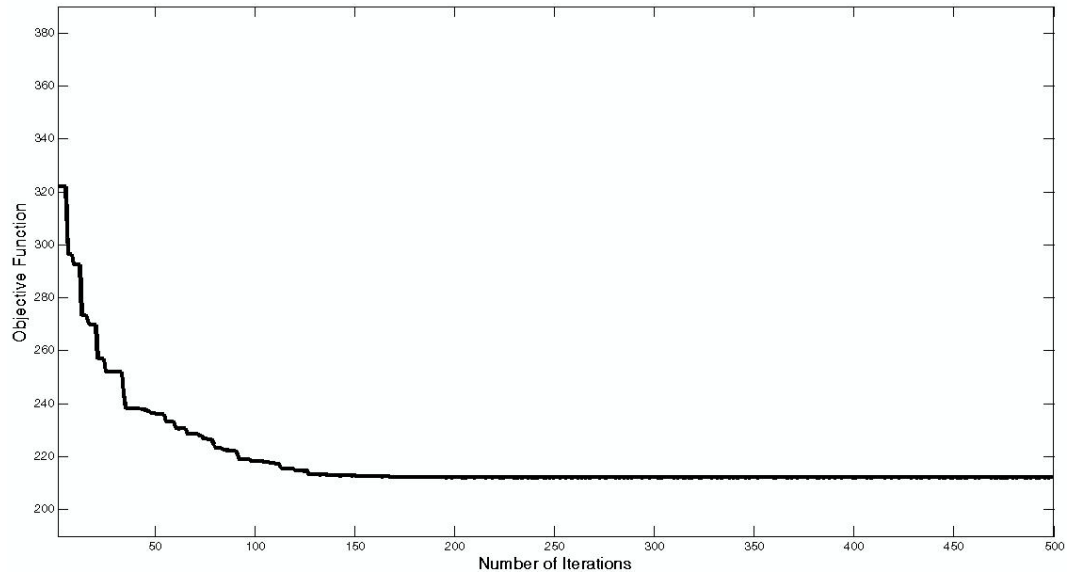

Figue 10. Convergence diagram for Variant 2, S235

Acknowledgement

This work has been supported by the Ministry of Education, Science and Technological Development of the Republic of Serbia, through the Contract for the scientific-research activity realization and financing in 2021, 451-03-68/2022-14/200102 and 451-03-68/2022-14/200108.

References

[1] PAVLOVIĆ,G., KVRGIĆ,V., SAVKOVIĆ,M., GAŠIĆ,M., ZDRAVKOVIĆ,N.: *The influence of the position of longitudinal stiffeners to the optimum dimensions of the box section of the single-girder bridge crane*, 3rd Conference on Mechanical Engineering Technologies and Applications "COMETa 2016", East Sarajevo – Jahorina, B&H, Republic of Srpska, pp. 131-138.

[2] QIN,D., ZHU,Q.: *Structural topology optimization of box girder based on method of moving asymptotes (MMA)*, International conference on intelligent computation technology and automation, Changsha, Hunan, China, pp.402–405.

[3] JARMAI,K., FARKAS,J.: *Optimum cost design of welded box beams with longitudinal stiffeners using advanced backtrack method*, Struct Multidisc Optim, 2001, 21, pp. 52–59.

[4] PAVLOVIĆ,G., SAVKOVIĆ,M., ZDRAVKOVIĆ,N., MARKOVIĆ,G.: *Optimal design for the welded girder of the crane runway beam*, Proc. Fifth International Conference Mechanical Engineering in the XXI Century MASING 2020, Niš, pp. 151-156.

[5] SAVKOVIĆ,M., BULATOVIĆ,R., GAŠIĆ,M., PAVLOVIĆ,G., STEPANOVIĆ,A.: Optimization of the box section of the main girder of the single-girder bridge crane by applying biologically inspired algorithms, Engineering Structures, 2017, 148, pp.452-465.

[6] WANG,P.F., DIAO,X.H.: Optimization design of the crane girder based on adaptive genetic algorithm, Advanced Materials Research, 2012, 591-593, pp.123-126.

[7] MILENKOVIĆ,B., JOVANOVIĆ,Đ.: *The Use of The Biological Algorithm in Solving Applied Mechanics Design Problems*, Scientific Technical Review, 2021, 71(1), pp.38-43.

[8] https://www.contrx.com/contrx-cranes/double-girder-bridge-cranes/

[9] OSTRIĆ,D., TOŠIĆ,D.: *Dizalice*, Faculty of Mechanical Engineering, Belgrade, 2005.

[10] SRPS U.E7.121/1986, 1986, Stability of steel constructions – Buckling of plates, Institute for standardization of Serbia, Belgrade.

[11] Petković, Z., Ostrić, D., 1996, Metalne konstrukcije u masinogradnji 1, Faculty of Mechanical Engineering, Belgrade.

[12] SRPS U.E7.081/1986, 1986, Stability of steel constructions - Axially compressioned steel members of constant cross section, Institute for standardization of Serbia, Belgrade.

[13] SRPS U.E7.086/1986, 1986, Stability of steel constructions – Effective lengths of compression members, Institute for standardization of Serbia, Belgrade.

[14] SRPS U.E7.101/1991, 1991, Stability of steel constructions – Lateral buckling of girders, Institute for standardization of Serbia, Belgrade.

[15] MIRJALILI,S.: Moth-flame optimization algorithm: A novel nature-inspired heuristic paradigm, Knowledge-Based Systems, 2015, 89, pp. 228-249.

[16] https://www.mathworks.com/matlabcentral/fileexchange/52269-moth-flame-optimization-mfo-algorithm

Received: 02.04.2022.
Accepted: 25.05.2022.

Analiza i optimizacija glavnog nosača mosne dizalice sa asimetričnim kutijastim poprečnim presekom

Predstavljeno istraživanje se bavi optimalnim projektovanjem glavnog nosača dvogredne mosne dizalice asimetričnog kutijastog poprečnog preseka. Algoritam moljca (MFO) se koristi za rešavanje ovog višekriterijumskog problema optimizacije. Ovaj algoritam je relativno nova metaheuristička metoda zasnovana na populaciji. U radu su kao funkcije ograničenja uzeti sledeći kriterijumi: čvrstoća, lokalna stabilnost limova (vertikalnih limova i gornje lamele), lokalna stabilnost uzdužnih ukrućenja, globalna stabilnost glavnog nosača, ugibi i period oscilovanja. Opravdanost predloženog postupka prikazana je na jednom primeru realnog rešenja dvogredne mosne dizalice. U ovom istraživanju ostvarene su značajne uštede u materijalu, u rasponu od 19,42 do 25,49 %. Upotreba ovog algoritma omogućava primenu veoma velikog broja varijabli i funkcija ograničenja, pri čemu se optimalne vrednosti dobijaju u relativno kratkom periodu.

Ključne reči: **Dvogredna mosna dizalica, Asimetrični kutijasti poprečni presek, Optimalno projektovanje, Metaheuristika.**